frontiers in Earth Science

ORIGINAL RESEARCH
published: 09 December 2021
doi: 10.3389/feart.2021.792504

Drainage Development in the Dunhuang Basin, NE Tibet, Controlled by Multi-Segment Fault Growth

Gan Chen[1,2,3], *Wenjun Zheng*[1,2,3]*, *Jingjun Yang*[1,2,3], *Lei Duan*[1,2,3], *Shumin Liang*[1,2,3], *Zhigang Li*[1,2,3], *Dongli Zhang*[1,2,3] and *Jianguo Xiong*[3]

[1]Guangdong Provincial Key Laboratory of Geodynamics and Geohazards, School of Earth Sciences and Engineering, Sun Yat-Sen University, Guangzhou, China, [2]Southern Marine Science and Engineering Guangdong Laboratory (Zhuhai), Zhuhai, China, [3]State Key Laboratory of Earthquake Dynamics, Institute of Geology, China Earthquake Administration, Beijing, China

The Dongbatu Shan (DBTS, also known as the Nanjie Shan), which interrupts the northern Tibetan foreland in the Dunhuang basin, is an active anticline. It has accommodated the northwestern growth of the eastern Altyn Tagh fault system (ATF). Although several thrust faults have been identified around the DBTS, their evolution history and influence on regional landscape have received little attention during the late-Quaternary. In this study, several geomorphic methods are used to investigate the interaction between drainage development and tectonic movement around DBTS. Based on high-resolution satellite images, field investigation, and cosmogenic nuclide ^{10}Be dating method, the fluvial landform sequences around DBTS were constructed. Using quantitative geomorphology methods including landscape relief profile, asymmetry factor (AF), and transverse topographic symmetry factor (T), we hypothesize that drainage deflection is controlled by multi-segment fault growth. Combining the results of the above-mentioned methods, we propose that Yulin He, flowing across the DBTS, had gone through several abandonments since the late mid-Pleistocene due to the lateral propagation of DBTS. Affected by the discharge of channel and multi-segment fault growth, our research confirms that the direction of river abandonment may have decoupled with the mountain range propagation trend. Based on the chronology dating, the DBTS has gone through two severe uplifts since ~208 ka and the shortening rate across the central DBTS is constrained to be ~1.47 mm/yr since ~83 ka. Given the fact that thrust faults are widely developed around DBTS, we propose that the flower-like structure formed by the northward growth of the eastern ATF could better explain the development of the secondary subparallel faults.

Keywords: drainage development, fault lateral growth, air gap, Dongbatu Shan (Nanjie Shan), Altyn Tagh fault

OPEN ACCESS

Edited by:
Rong Yang,
Zhejiang University, China

Reviewed by:
Gang Rao,
Southwest Petroleum University, China
Haopeng Geng,
Lanzhou University, China

***Correspondence:**
Wenjun Zheng
zhengwenjun@mail.sysu.edu.cn

Specialty section:
This article was submitted to Quaternary Science, Geomorphology and Paleoenvironment, a section of the journal Frontiers in Earth Science

Received: *10 October 2021*
Accepted: *18 November 2021*
Published: *09 December 2021*

Citation:
Chen G, Zheng W, Yang J, Duan L, Liang S, Li Z, Zhang D and Xiong J (2021) Drainage Development in the Dunhuang Basin, NE Tibet, Controlled by Multi-Segment Fault Growth. Front. Earth Sci. 9:792504. doi: 10.3389/feart.2021.792504

INTRODUCTION

The mechanism and kinematics of mountain ranges controlled by fault lateral growth had been a major concern for researchers due to their implications on seismic hazards and hydrocarbon reservoirs (Hetzel et al., 2004; Lacombe et al., 2007; Ramsey et al., 2008; Bretis et al., 2011; Ellis and Barnes, 2015). Drainage networks are sensitive to the surface slope and thus have been used to quantify how tectonic movement controls landform evolution (Keller et al., 1998; Ramsey et al., 2008;

Keller and DeVecchio, 2013). Six landscape criteria were proposed as indications of the propagation of fault-related folds developing above active faults by Keller et al., 1999. Follow-on research suggests that three criteria among them provide the strongest evidence: 1) deformation of progressively younger landforms (Jackson et al., 2002; Bennett et al., 2005); 2) a series of elevation decreased air (wind) gaps (Hetzel et al., 2004; Ramsey et al., 2008); and 3) development of inherited drainage patterns (Ramsey et al., 2008; Keller and DeVecchio., 2013). When the fold lateral propagations happen, tectonic tilting towards the propagating direction would affect the development of drainage basin asymmetry (Schumm et al., 2000; Burbank and Anderson, 2001). Asymmetry factor (AF) (Hare and Gardner, 1985) and transverse topographic symmetry factor (T) (Cox, 1994) are two common quantitative geomorphology indexes used to evaluate drainage basin asymmetry, which have been proven as good indications of tectonic movement in southern Iberian Massif and Taiwan (Salvany, 2004; Ramsey et al., 2007). In addition, many analogue and numerical models also display that curved air gaps could indirectly record fold lateral growth (Grasemann and Schmalholz, 2012; Collignon et al., 2015). However, if we only use a single criterion to detect fold lateral growth, the result could be unreliable and misleading. Therefore, a combination of different geomorphological constraints is needed to distinguish passive exhumation and active fold growth (Burbank and Anderson, 2001).

The Altyn Tagh fault system (ATF), a 1,500 km long sinistral strike-slip fault system that forms a boundary for the Tibetan plateau to the north, plays an important role in accommodating the continental deformation produced by the India/Asia collision (Molnar and Tapponnier, 1975; Avouac and Tapponnier, 1993; Cowgill et al., 2000; Tapponnier et al., 2001; Yin et al., 2002). The style and strike-slip rate of faulting have been a major concern of researchers over the last 3 decades, and till now studies have generally stated that there is a gradual decrease from ~10 ± 2 to 0 ± 2 mm/yr along the eastern section of the ATF (Xu et al., 2005; Cowgill, 2007; Zhang et al., 2007; Cowgill, 2009; Gold et al., 2009; Zheng et al., 2013; Liu et al., 2020). Nevertheless, two main questions derived from the kinematics of the ATF along the north of the eastern end still remain unsolved: 1) how did the fault evolve and 2) what kind of landscape was formed by the movement of ATF? Dongbatu Shan (DBTS) faults, developed in the north pediment of the eastern ATF, is regard as the secondary fault of ATF, and expresses thrust conditions with a sinistral component (Cunningham et al., 2016). Although the magnetotelluric method can provide the fault geometry in depth (Xiao et al., 2011; Xiao et al., 2015; Xiao et al., 2017; Li et al., 2020), and active fault studies reveal fault distribution and activities during the late-Pleistocene (Chen et al., 2020; Yang et al., 2020), the published dataset is not good enough to comprehensively answer how the tectonic activities around DBTS controlled drainage development during the late Quaternary.

In this study, due to the abundant drainages and various kinds of fluvial landforms developed around DBTS, we aim to determine: 1) the geomorphic sequences of landscapes by satellite image analysis, field investigation, and beryllium-10 (^{10}Be) terrestrial cosmogenic nuclides dating; 2) the features of the topography profile along the mountain crestline, drainage pattern, and geomorphic indexes (AF and T); and 3) the landform's evolution and its implication in the regional tectonic movement.

GEOLOGICAL AND TECTONIC SETTING

The Dunhuang basin, located in the northeastern Tibetan plateau, is bounded by the Altyn Tagh fault (ATF) to the south (**Figure 1B**). The basement of the basin belongs to the Paleozoic Dunhuang Orogenic Belt that consists of Archean-Proterozoic rocks, including high-grade tonalite-trondhjemite-granodiorite gneisses, amphibolite, and widespread granite intrusions of the Hercynian period (He et al., 2013; Zhao et al., 2015; Wang et al., 2017). Two mountain ridges composed of the basement rocks, i.e., the Sanwei Shan and Dongbatu Shan, divided the eastern Dunhuang basin into three sub-basins: the Daba, Tashi, and Anxi basins (**Figure 1B**). Jurassic, Cretaceous, and Neogene strata overlay the basement rock with an unconformable contact (Zhuang et al., 2011). With a north-tilted slope, Quaternary conglomerates have been transported by numerous drainages and fulfilled the sub-basins (Wang, 1989). According to the published geological map, the conglomerates can be distinguished into five phases, named Fan1 (early-Pleistocene), Fan 2 and Fan3 (mid-Pleistocene), and Fan4 and Fan5 (late-Pleistocene), respectively (**Figure 1C**).

We focus on the Dongbatu Shan (DBTS) in this study. It strikes east-west with a length of ~100 km and a width of ~10 km. The DBTS, which is believed to have developed no earlier than the early Quaternary (Wang, 1989; Cunningham et al., 2016; Yang et al., 2020), is 100–300 m higher than the surrounding bajada. The uplift and landscape of the DBTS are controlled by several south and north dipping thrust faults, which are possibly reactivations of older fabrics (Cunningham et al., 2016). Based on chronometric dating of the alluvial fans and fluvial terraces, fault scarps and active folds in the western and eastern of the DBTS are found to have been developed during the late-Pleistocene (Chen et al., 2020; Yang et al., 2020). The movement of the DBTS fault in the eastern end has largely affected the asymmetric development of the Shule alluvial fan (Wang et al., 2004). During the Holocene, the activity of the faults around the DBTS remains unclear.

DRAINAGE FEATURES AROUND THE DBTS

Based on bedrock exposure, the DBTS can be divided into three structural domains, namely DBTS-W, DBTS-C, and DBTS-E from west to east, respectively (**Figure 2B**). The Yulin He (the river of Yulin), deflecting towards the west, flows across the western nose of DBTS-C and the eastern nose of DBTS-W, forming a series of fluvial terraces on both sides of the river since the late-Pleistocene (Chen et al., 2020). Several drainages have incised DBTS-W and the river flow turns into groundwater

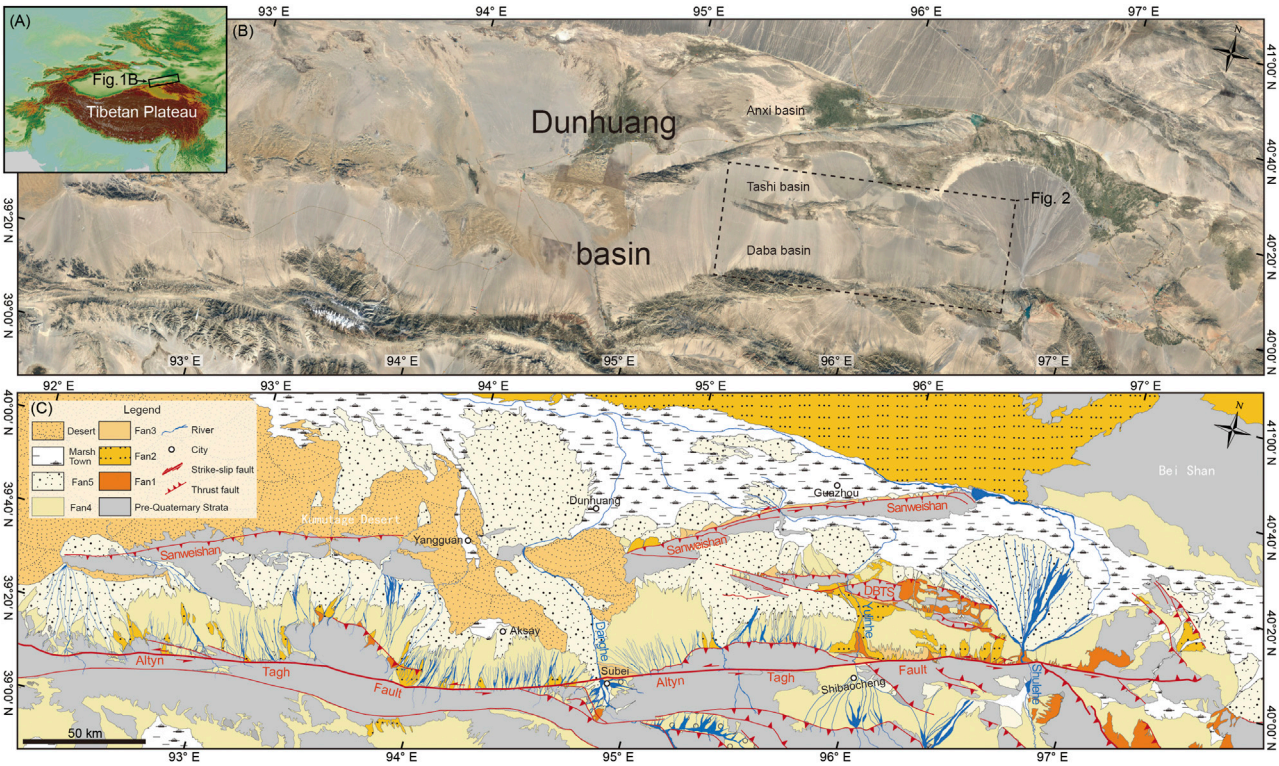

FIGURE 1 | Geomorphic map of the Dunhuang basin. **(A)** Topographic map of the Tibetan plateau. **(B)** Google earth satellite imagery showing the geomorphic features of Dunhuang basin and its surrounding area. **(C)** Interpretation map showing the distribution of Quaternary sediments and active faults around the Dunhuang basin. Active fault locations are modified from "Map of active faults in China" and "Map of active faults in northern Tibet" by Deng et al., 2003 and our own observation.

as it comes into the basin floor. In DBTS-C, paleochannels with a similar scale can be seen on the mountain crestline and the southern alluvial fan. Hanxia and Wudaogou, which had incised across the eastern DBTS-C, are now dry valleys (seasonal channels). In DBTS-E, groundwater overflowed through the Daba basin and then incised across the western and eastern noses of the anticline. Interestingly, seasonal channels around Dushanzi show a dendritic pattern which seems similar to the present Yulin He and paleo-channel preserved on the mid-Pleistocene alluvial fans and mountain crestline.

Field photographs indicate the clear groove shape of air gaps (AG) and water gaps (WG) along the mountain crestline of DBTS-C (**Figure 3A**). The paleo-riverbed of AG2, ~300 m wide, is relatively flat with rounded fluvial conglomerate preserved on it (**Figure 3B**). Paleo-terrace T1 can be found on the western bank (**Figure 3C**). Huge, rounded bedrocks, small rounded fluvial conglomerates reflecting strong hydrodynamic conditions (**Figure 3D**), and fluvial conglomerates preserved on the riverbed of AG3 were observed (**Figure 3E**). At the eastern bank of the Yulin He on the mountain crestline, rounded fluvial conglomerate can also be found on the platform which is ~100 m higher than the present river (**Figures 3F,G**). All these phenomena indicate that paleo-Yulin He had flown across DBTS-C, and were then abandoned due to fault evolution.

METHODS

Mapping Fluvial Landscapes

The landform sequences and distribution are the basis of exploring landscape evolution during different time stages. Due to the absence of vegetation on the surface of landforms in our research area, we can clearly identify different landforms on the satellite images. Combined with field investigation, worldview satellite image with a resolution of 0.5 m was used to distinguish landform sequences and distribution around DBTS. Landform distinguishing was mainly based on the degree of surface erosion and the height above the modern Yulin He. Based on the Shuttle Radar Topography Mission (SRTM) DEM (30 m-resolution), we extracted six topographic profiles along the mountain ridge and alluvial fans. The profiles could help us better distinguish the sequence of alluvial fans and Paleochannels. Two topographic profiles orthogonal to the fault strike are extracted to calculate the amount of fault vertical uplift.

Dating Geomorphic Surfaces

The chronology dating of the geomorphic surface is the most effective way to constrain the process of landscape evolution. We use *in situ* cosmogenic nuclide ^{10}Be dating method to constrain the abandonment ages of Paleo-channels and Paleo terrace. The ^{10}Be dating method hypotheses that ^{10}Be nuclide concentration

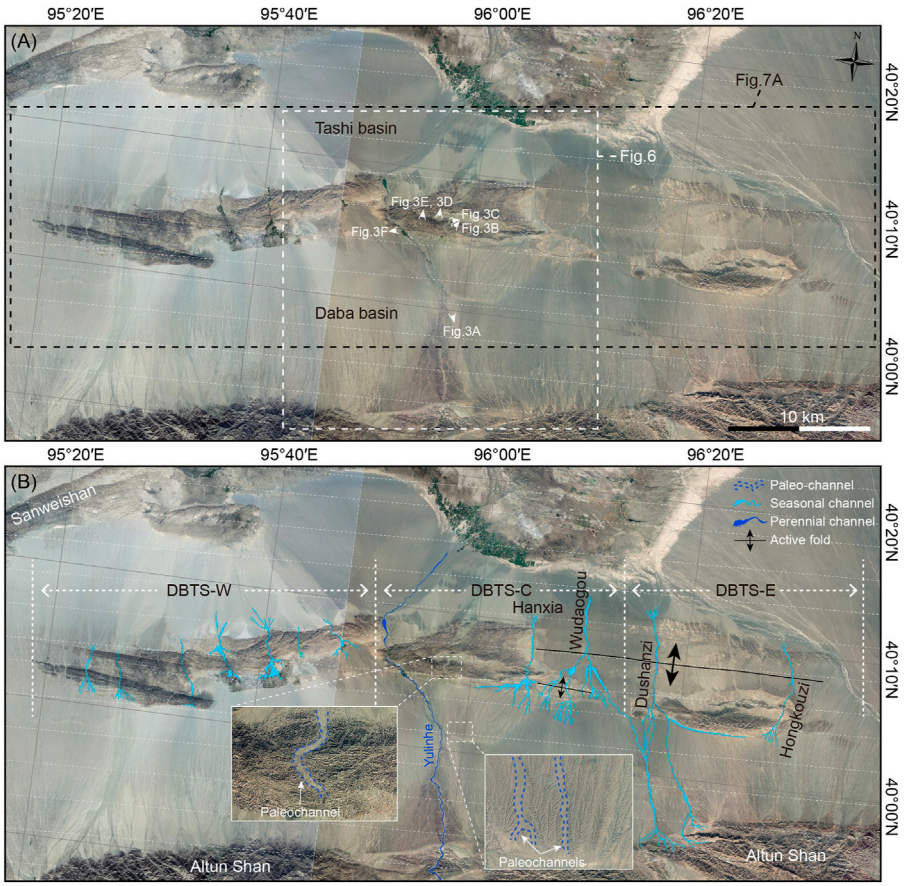

FIGURE 2 | (A) CIRS-P5 satellite images (2.5 m-resolution) around the DBTS. **(B)** Drainage distribution around the DBTS. White dashed lines depict the geographical divisions of DBTS-W, DBTS-C, and DBTS-E.

would accumulate since the riverbed abandoned quartz-rich pebbles exposed to cosmic rays (Gosse and Phillips, 2001). If the inherited nuclide concentration before the riverbed abandoned can be obtained, we could subtract it from the total nuclide concentration to calculate the exposure ages. In the field, we have found that many quartz-rich and sub-round gravel pebbles are well preserved on the surface of the riverbed and terrace at AG2 and AG3 (**Figure 4**). These pebbles, with diameters of ~1–3 cm, are suitable for ^{10}Be dating method to constrain the abandonment age of paleo-channels. At AG2, two superficial ^{10}Be samples are collected, one from the surface of riverbed (YLH-16) and the other from the T1 (YLH-15) (**Figures 4A,B**). At AG3, one superficial ^{10}Be sample is collected on the surface of the riverbed (YLH-17) (**Figure 4C**). We suspect that the inherited nuclide concentration of the paleo-channels is approximately the same as the terrace formed in the Late-Pleistocene incised by Yulin He, which has been simulated by Chen et al., 2020. The pre-process of these samples is performed at the Key Laboratory of the Institute of Crustal Dynamics, China Earthquake Administration (Chen et al., 2020). The ^{10}Be/^{9}Be ratio is tested at CEREGE (Le Centre Européen de Recherche et d'Enseignement des Géosciences de l'Environnement, Laboratoire de Tectonique). After subtracting the inherited nuclide concentration, the CRONUS-Earth online calculator (Balco et al., 2008) (http://hess.ess.washington.edu) and the time-independent scaling model of (Lal, 1991) and (Stone, 2000) are used to calculate the abandonment age of each landform. Dating results are shown in **Table 1**.

Analyzing Drainage Development

If the lateral growth had happened along the strike of DBTS, evidence could have been recorded on drainage development. **Figure 5A** is an idealized cartoon model showing the development of the present river and drainages influenced by the propagating anticlines through time. Fan-shaped drainages form perpendicular to contours on the fold and one river flow across the fold tip at stage I before lateral propagation. With fold propagation along strike (stage II), newly formed drainages are perpendicular to contours, while some deep incised channels formed at stage I may have inherited their curved pattern. These channels, which are not normal for the contours and sometimes nearly parallel to the mountain ridge, are named as "inherited drainages" or "forked drainage" (Keller et al., 1999; Ramsey et al., 2008; Bretis et al., 2011). If the incision rate of the western river can keep pace with the uplift rate, the river would incise a gorge through the nose of the fold (**Figure 5A**). Accompanied by the

FIGURE 3 | Photographs showing paleo-channel geomorphology characters around DBTS. Locations are marked in **Figure 2B**. **(A)** Concave pattern along the mountain crestline showing air gaps and water gaps. **(B)** and **(C)** Paleo-riverbed and terrace T1 at AG2. **(D)** Tributary paleo-river on the top of the mountain. **(E)** Paleo-riverbed of AG3. **(F)** and **(G)** Platforms that are preserved on the eastern bank of the present Yulin He.

consistent fold propagation (stage III and IV), when the river incision rate cannot keep up with the uplift rate, the outlet may be abandoned, leading the river to form a new gorge through the nose of the fold. The abandoned outlet left on the mountain ridge is named AG and the present river gorge is WP (water gap). In such hypotheses, WP represents the nose of the fold and the air gap represents the nose of the fold before propagation. Thus, we could see a decrease in elevation of WPs along the mountain ridge relief (**Figure 5B**). Where such a pattern is recognized, fold lateral propagation could be the likely cause (Keller et al., 1999; Ramsey et al., 2008; Keller and DeVecchio, 2013). Based on the SRTM DEM (30 m resolution), we extract the drainage map of different segment of DBTS to detect inherited channels.

In order to analyze the type and amount of asymmetry of the drainage basins on DBTS, we use two quantitative geomorphic indexes: AF (Hare and Gardner, 1985) and T (Cox, 1994). These two methods are all based on the deflection of the trunk river which may be influenced by

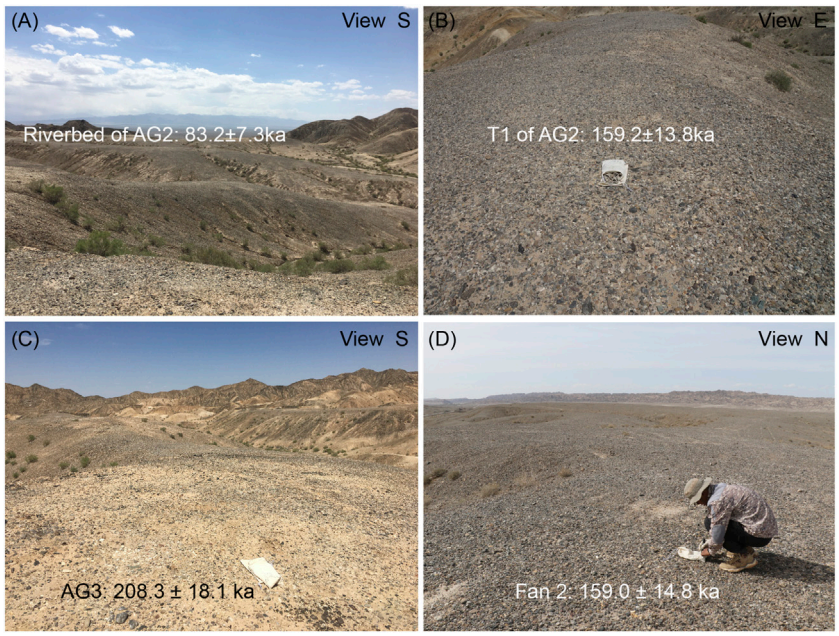

FIGURE 4 | Field photographs showing ^{10}Be samples collected on the surface of **(A)** AG2, **(B)** paleo-terrace T1 at AG2, **(C)** AG3, and **(D)** Fan 2.

tectonic tilting. As different types and different periods of landform are mostly distributed around DBTS-C, we use these two methods to further analyze the drainage basin asymmetry and tectonic information.

The AF—index describes the asymmetry of a drainage basin. It is calculated by AF = 100 (A_r/A_t), where A_r represents the drainage area to the right of the trunk stream towards downstream and A_t is the area of the drainage basin (**Figure 5C**). If the AF is 50 the drainage basin is symmetrical, while if the AF is more or less than 50 this represents the asymmetry of the drainage basins (Ramsey et al., 2007). In this study, an AF > 50 would imply the trunk river is migrating westwards, and conversely an AF < 50 would imply the trunk river is migrating towards the east. We calculate the AF for each of the ten basins in the north of DBTS ridge, and present the results in **Table 2**.

The T - index is used to quantify the amount of asymmetry of the main stream within a drainage basin and how the asymmetry varies in length (**Figure 5C**). We divided the main stream into 300 m for each segment in this study. For each segment, T is the ratio of the distance from the basin midline to the active main stream (Da) and to the basin divide (Dd); T = Da/Dd. If the basin is symmetrical, Da = 0 and T = 0. The asymmetry would increase as the T values approach 1. For each segment, it can be seen as a two-dimensional vector with a length equivalent to Da/Dd, and a direction (bearing) perpendicular to the segment that indicates movement of the segment with regard to the basin midline. We used a MATLAB based toolbox—TecDEM (Shahzad and Gloaguen, 2011) to calculate the value of T and bearing. The mean value of T and bearing could represent overall deflection of the main stream in each drainage basin. The results of this are shown in **Table 2**.

RESULTS

Landform Features and Sequences Around DBTS

Our previous work has identified ten major fluvial terraces developed within alluvial fans along the Yulin He during the late-Pleistocene (Chen et al., 2020). In this work, we extend the research area to collectively cover the overall area around DBTS. To the south of DBTS, mid-Pleistocene alluvial fan (Fan 2) is widely distributed (**Figures 6A,B**) and forms the top surface of the Daba sub-basin (**Figures 6C–E**). Early-Pleistocene alluvial fan (Fan 1) developed beneath it, and is mainly exposed near the mountain front of DBTS and Altun Shan. Late-Pleistocene alluvial fan (Fan 3) is formed in the north of DBTS, which is abandoned at ~30.7 ka (Chen et al., 2020). Five thrust faults, surrounding DBTS, striking approximately west-east direction, are named F1 to F5, respectively. Influenced by the uplift of DBTS-W, the surface of Fan 2 expresses a significantly southward tilting in the south of DBTS-W (**Figure 6F**).

In DBTS-C, the present Yulin He flows across its western nose, and one dry valley-Hanxia incised across its eastern nose (**Figure 7A**). Four possible air gaps exist along the crest DBTS-C (**Figure 7B**). Among them, air gap 2 (AG2), with westward deflection, has the largest scale at ~1,500 m wide and over 70 m deep, while the other air gaps are only 300–500 m wide and ~30 m deep. Topographic profile crossing the AG2 shows that paleo-terrace T1 is ~10 m higher than the Paleo-riverbed (**Figure 7C**). The abandonment age of the riverbed is determined to be 83.2 ± 13.8 ka after eliminating the inherited ^{10}Be concentration (**Figure 4A**), and terrace T1 is 159.2 ± 13.8 ka (**Figure 4B**). Higher possible paleo-terraces cannot be clearly defined as no fluvial conglomerate was

TABLE 1 | Calculating ^{10}Be exposure ages.

Sample ID	ID	Latitude	Longitude	Elev (m)	Depth (m)	Dissolved mass (g)	Carrier mass (mg)	Corrected ^{10}Be/^{9}Be	^{10}Be concentration (atoms g^{-1})	Error (atoms g^{-1})	Inheritance ^{10}Be concentration (atoms g^{-1})	Error (atoms g^{-1})	Age (ka)	Error (ka)
YLH-14	Fan 2	40.050	95.950	1791	0	30.04	0.22	5.8534E-12	2.80E+06	4.76E+04	3.85E+05	+9.93E+04	159.0	14.8
YLH-15	T1	40.095	95.956	1830	0	30.17	0.21	5.9814E-12	2.84E+06	6.51E+04		–5.47E+04	159.2	13.8
YLH-16	AG2	40.094	95.960	1820	0	31.39	0.22	3.56774E-12	1.68E+06	4.49E+04			83.2	7.3
YLH-17	AG3	40.101	95.917	1818	0	26.32	0.22	6.29374E-12	3.36E+06	7.53E+04			208.3	18.1

preserved. To the west at AG3, the abandonment age of the riverbed is 208.3 ± 18.1 ka (**Figure 4C**). Several paleochannels, with similar scales to the present Yulin He, are preserved on the surface of Fan 2 in the southern DBTS. The central alluvial Fan 2 has a convex-up shape shown by topographic profiles P1 to P4 (**Figure 7D**). Along the western segment of Fan 2, some ~10 m higher fan surfaces exist and were abandoned at 159.0 ± 14.8 ka (**Figure 4D**, Chen et al., 2020). The longitudinal profile of AG2 shows a convex shape of the paleo-riverbed and the amount of uplift made by F2 is constrained as ~103 m (**Figure 7E**). For the fault scarp of F4, the vertical displacement is estimated to be 28 ± 2 m (**Figure 7F**).

Drainage Characters on the Flank of DBTS

The drainage network pattern shows some differences in three different segments of DBTS. In DBTS-W, seven major rivers have incised through the mountain and split it into many small segments (**Figure 8A**). The newly formed drainages surrounding the hills in all aspects may have covered the inherited drainages so that we could not observe them. As nearly no terrace was preserved along these gorges, it is difficult to limit the time when the river cuts through the DBTS-W. In DBTS-C, many instances of fan-shaped drainage are overprinted by secondary tributary and formed relatively larger drainage basins on the northern flank of DBTS-C. The tributary pattern on the south flank of DBTS-C is similar to the idealized pattern shown in **Figure 5A** and four inherited drainages are clearly identified (**Figure 8B**). The pattern of drainage network on DBTS-E also shows an idealized pattern so that the inherited drainage approximately parallel to the mountain crestline can be observed (**Figure 8C**).

The results of AF are a great indication of the mountain inclination (**Figure 9A**). Basin 5 to 10 have an AF of 55 to 30 and show a steady decrease in the east direction, indicating an eastern inclination of DBTS-C. But the AF of basin 1 to 5 display an arbitrary value. The AF value of basin 1 and 4 is lower than 50, while basin 2 and 3 is higher. We state that the disordered AF may be affected by the uplift of DBTS-W, which is also shown in the value of T.

The mean value and bearing of T of basin 6 to 10 shows a uniform eastern migration of all trunk rivers (**Figures 9B,C**). Basins 1, 2, and 4 have T of 0.18, 0.14, and 0.27 respectively, and bear towards the southeast. Basins 3 and 5 have T of 0.30 and 0.24, and bear towards the southwest. We believe this phenomenon is influenced by the uplift of the western mountain DBTS-W. In summary, both the value of AF and F seem to be reasonably explained by tectonics.

DISCUSSION

Restoration of Landform Evolution Induced by Fault Growth

The distribution and chronology of different landforms, drainage patterns, and quantitative morphometric indexes help us to establish the landform evolution around DBTS. Based on the inherited drainage pattern, we suggest fold lateral propagation

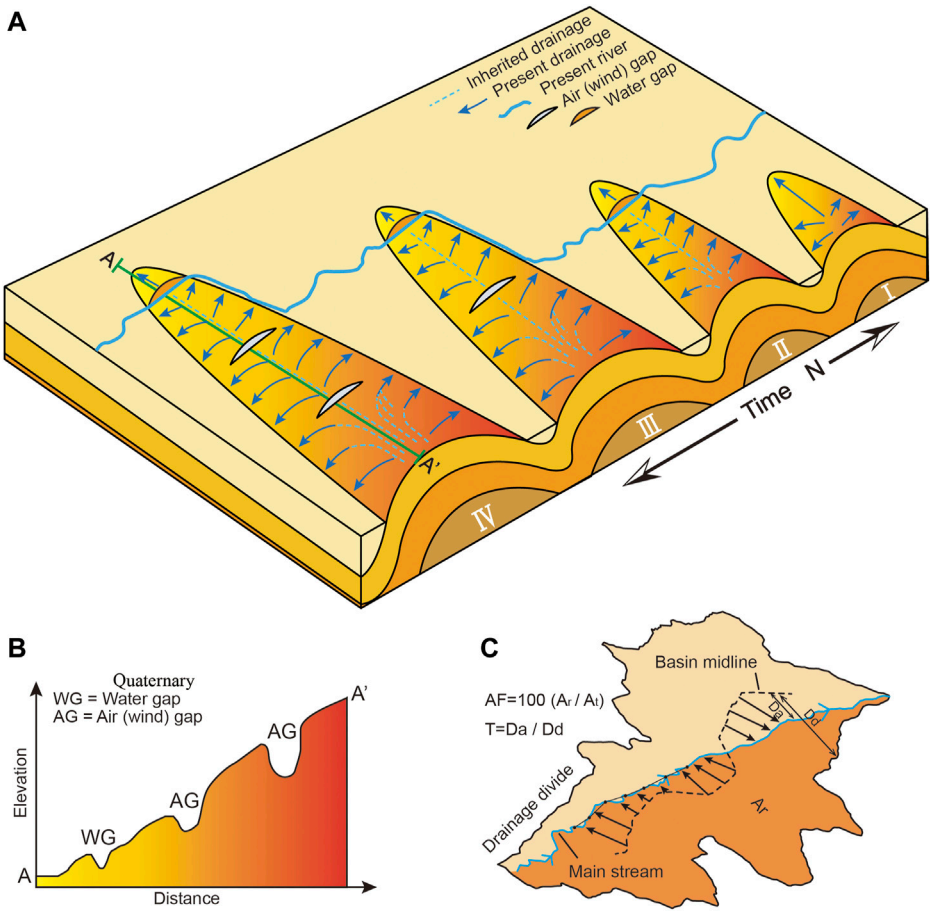

FIGURE 5 | Three conceptual models showing the drainage development controlled by fold lateral propagation. **(A)** A cartoon illustrating fan-shaped drainages on the flanks and river flow across the western nose of a growing fold. At stage II, the fold propagates towards the west. Inherited channels (dotted lines) may be preserved on both flanks of the fold. The incision rate of the western river can keep up with the fold uplift and incised a gorge across the fold nose. At stage III, the western river cannot catch up with the fold uplift such that the gorge is abandoned, leaving one wind gap. A new river would migrate to a new course where it can be incised through. At stage IV, more air gaps are preserved on the mountain crestline due to fold propagation (modified from Ramsey et al., 2008). **(B)** Topographic profiles across the propagating fold crest showing air (wind) gap features (modified from Keller et al., 1999). **(C)** An example of the methods used to calculate asymmetry factor (AF) and transverse topographic symmetry factor (T) of a drainage basin (modified from Cox, 1994; Salvany, 2004).

TABLE 2 | Morphometric values obtained from DBTS-C.

Drainage basin	Asymmetry factor (AF)	Transverse topographic symmetry factor	
		Mean T	Mean bearing
1	45	0.18	133
2	53	0.14	158
3	58	0.30	173
4	43	0.27	157
5	55	0.24	197
6	40	0.13	124
7	32	0.42	157
8	36	0.20	96
9	32	0.47	112
10	30	0.44	120

occurred on DBTS-C and DBTS-E. Combining the terrace deformation with ^{10}Be exposure age, the shortening rate across the west nose of DBTS-E is constrained to be ~0.3 mm/yr since ~50 ka (Yang et al., 2020). At DBTS-C, the value of AF and T show a clear drainage migration towards east active, indicating an eastward titling. To the west flank of DBTS-C, as fault scarp that

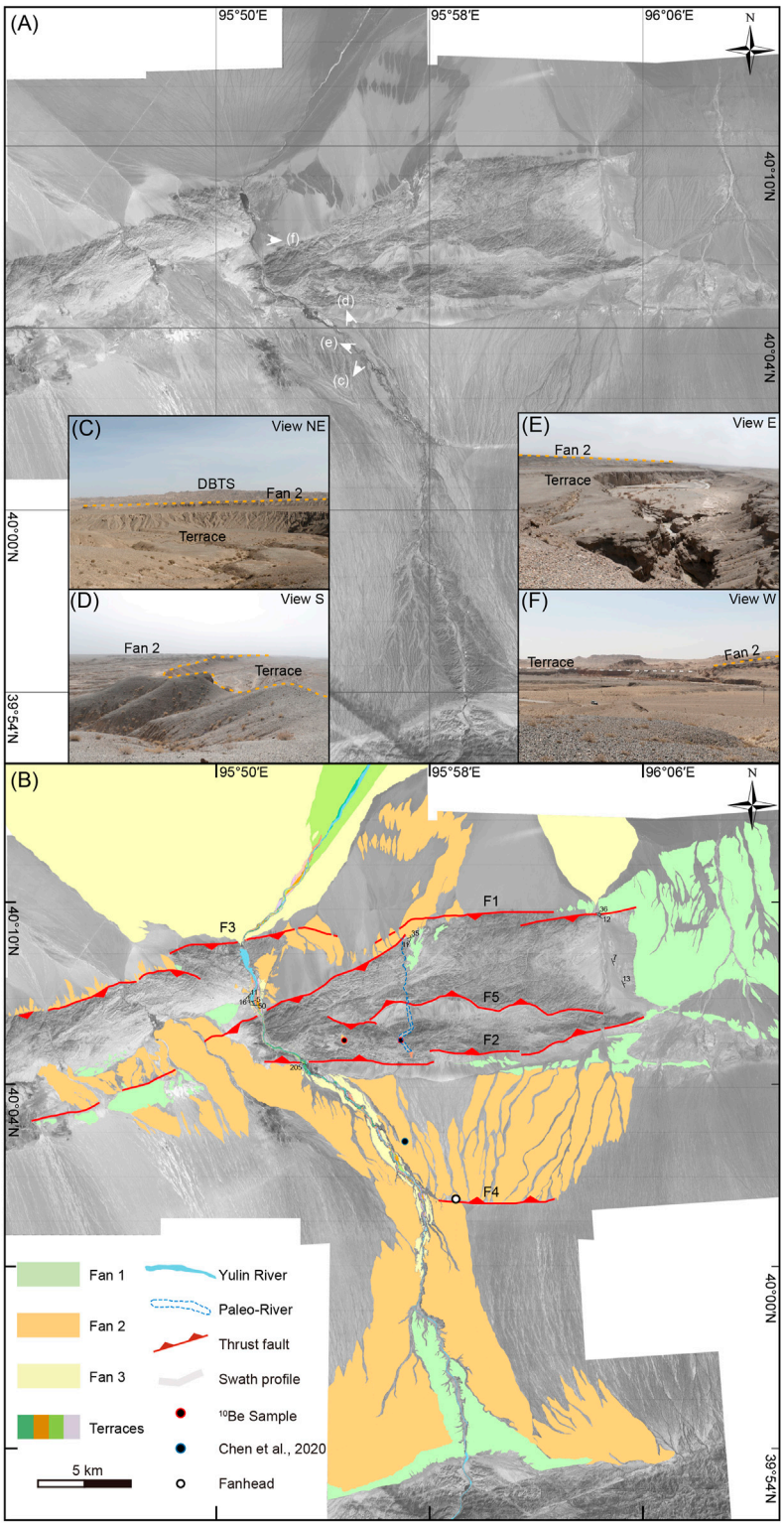

FIGURE 6 | Landform style, sequences, and distribution around DBTS-C. **(A)** Worldview image with 0.5 m-resolution showing the geomorphic feature of the research area. **(B)** Interpretation of the distribution and sequences of drainage landforms. **(C,D)**, and **(E)** Field photographs showing the contact relationship of terraces and alluvial Fan 2 along the upstream of the Yulin He. **(F)** Southward tilting of Fan 2 developed in the south of DBTS-W. Photograph positions are marked in **(A)**.

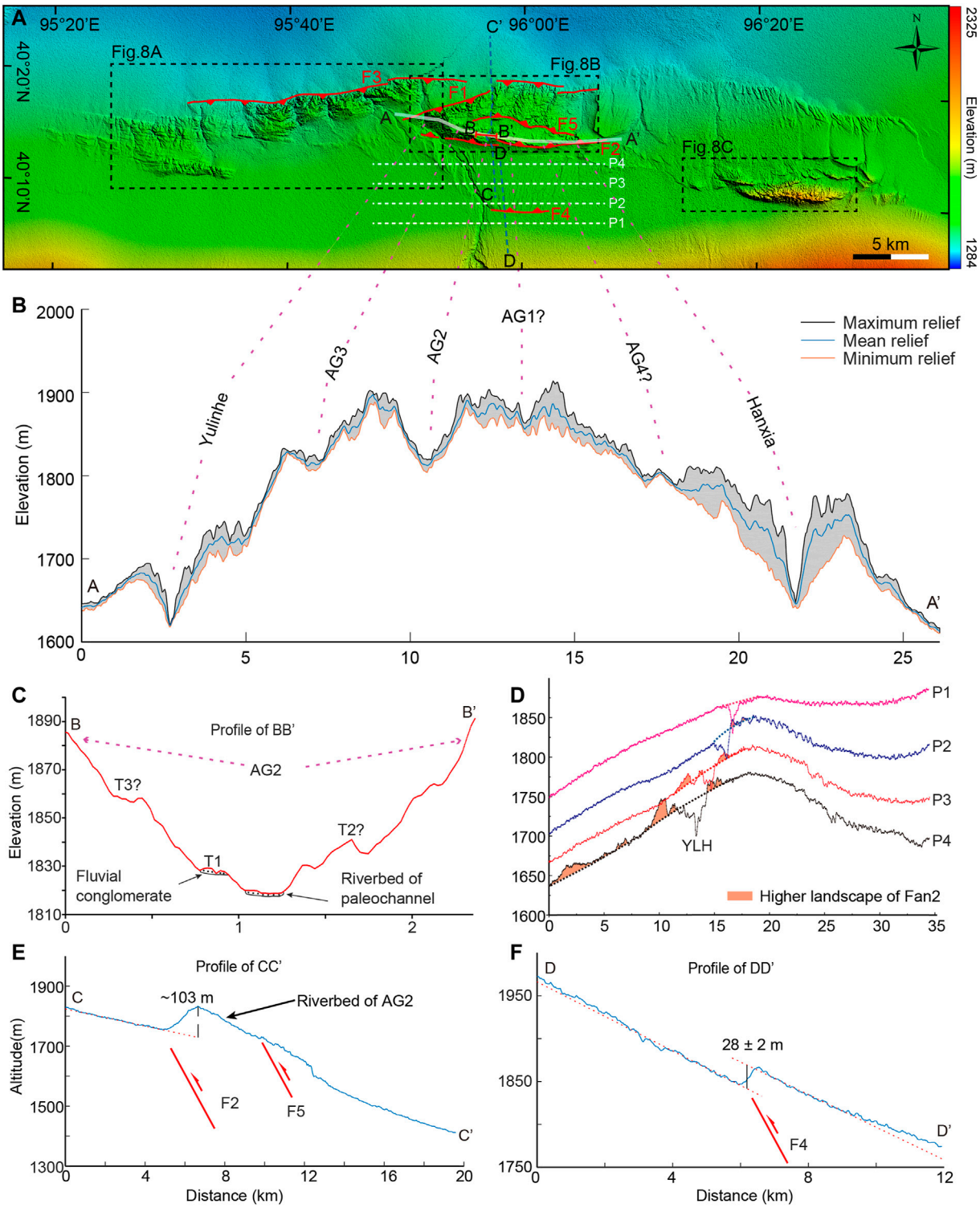

FIGURE 7 | Topographic feature of landscapes around the DBTS. **(A)** Topographic map of DBTS (superimposed on the 30 m-resolution Shuttle Radar Topography Mission DEM; https://lta.cr.usgs.gov/SRTM). **(B)** Topographic profiles along the mountain crestline of DBTS-C. **(C)** Cross profiles of AG2. **(D)** Four relief profiles across Fan 2 in the south DBTS-C. **(E)** and **(F)** Topographic profiles of F2 and F4 fault scarps.

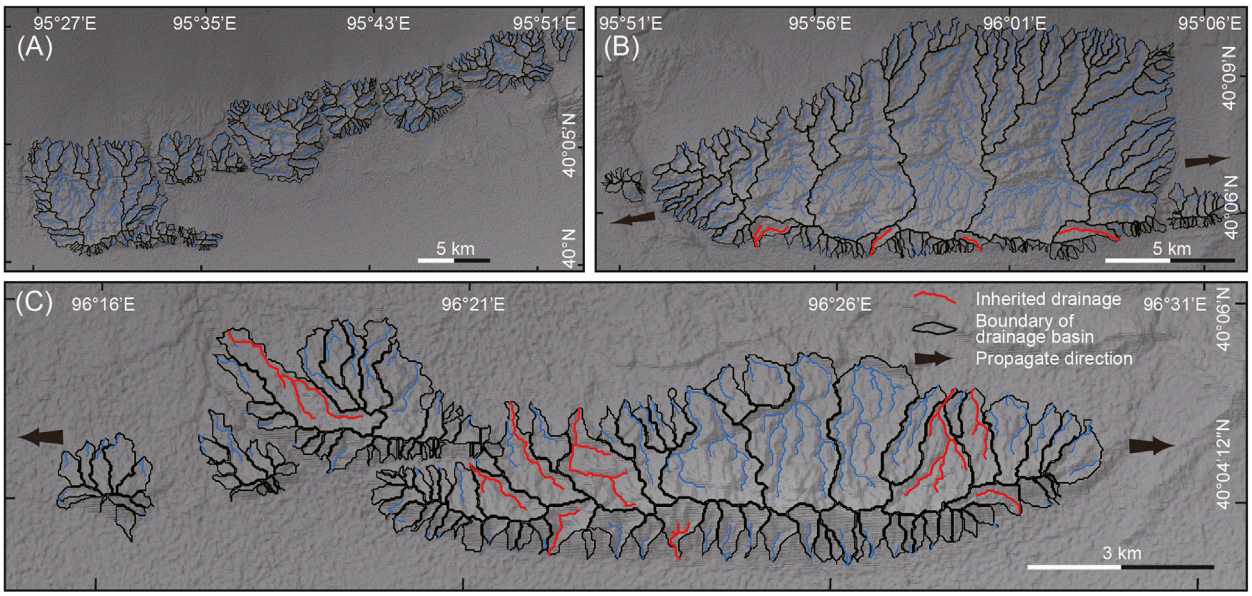

FIGURE 8 | Drainage patterns of the **(A)** DBTS-W, **(B)** DBTS-C, and **(C)** DBTS-E extracted from the 30 m SRTM DEM. Red line represents the inherited drainages.

displaced the alluvial Fan 2 can be clearly observed in the east end of DBTS-W (**Figure 6B**); these two domains have overlapped together. The disordered value of AF and T could reveal the fold superimposition that the uplift of DBTS-W would influence the westward propagation of DBTS-C. Yang et al., 2020 propose that fault uplift of DBTS-W had displaced the alluvial fan at the western end since ~46 ka and may have connected with Sanweishan fault (Cunningham et al., 2016). In the center of DBTS-W, we found the metamorphic rock are thrust on the early-Pleistocene conglomerate, indicating early activity of the fault (Chen et al., 2020). Thus, we regard that the late-Pleistocene fault movement at the east and west end of DBTS-W could indicate a fault lateral growth. In summary, the above evidence reveals that the three segments of DBTS could have gone through east-westward propagation during the late Quaternary. If this supposition is correct, much more evidence would have been recorded on other landforms that surround DBTS.

Under normal conditions, the paleo-river would migrate to AG3 when the AG2 was abandoned. Curiously, the abandonment age of the riverbed at AG3 is ~208.3 ka, which is older than T1 of AG2. The capability of river incision may be influenced by lithology, discharge, and topography relief (Burbank and Anderson, 2001). Since the lithology of DBTS is consistent along the strike, we can exclude the impact of lithology change on river abandonment. Observed from the present mountain crestline relief, the elevation of AG3 is similar with AG2 (**Figure 7B**). As mentioned in the previous paragraph, the uplift of the east end of DBTS-W could influence the topography of the western flank of DBTS-C that could make the riverbed of AG3 higher than AG2 at early stages. The height differences between mountain crestline and sub-basin of DBTS-W and DBTS-C are ~150 and ~200 m, respectively. The higher topography of DBTS-C could reveal a stronger uplift. Then, with the stronger uplift of the DBTS-C, the elevation of AG2 would arise and gradually keep up with AG3. In addition, the scale of AG3 is much smaller than AG2, indicating a weaker incision capability. Thus, we suppose AG3 would be abandoned earlier due to relatively weak hydrodynamics and higher topography. Leading to the acquisition of the abandonment age of Paleo-terrace T1 agreeing well with Fan 2, they may be the same landform and connected before ~160 ka. During that time, river incision could have kept up with mountain uplift and gradually incised the alluvial fan and the bedrock of DBTS to form T1. Until ~83 ka, river incision could not keep up with the mountain uplift of the riverbed of AG2 and river flow on the surface of Fan 2 was abandoned, as the height difference between paleo- T1 and riverbed is the same with the height difference revealed on Fan 2 (**Figures 7C,D**). The present Yulin He has evidently deflected towards the west near fault F4, indicating the uplift of F4 has largely affected the evolution of paleo-rivers. We believe the river would have merged into the present channel of the Yulin He since ~83 ka, where the oldest fluvial terrace found is ~42.8 ka (Chen et al., 2020).

Based on the chronology and topographic data, we had analyzed evolution sequences of the paleo-channels of Yulin He. However, whether the evolution of Yulin He is a single river swinging around or multiple tributaries gradually abandoned needs further discussion. According to the drainage pattern and topographic profile relief, we determined the location of apex of Fan 2 (**Figure 6B**), which corresponds to the position of water outlet in front of the Altun Shan. The phenomenon shows that the upstream position of Yulin He has not changed since Fan 2 was accumulated. Field investigation has found terraces ~100 m higher than the modern riverbed, preserved on the east bank of the Yulin He. Topographic profile of AG2 also shows some possible terraces exist (**Figure 7C**). These phenomena may indicate that paleo-channels of Yulin He may have once flown across these paleo-channels at the same time. In consideration of the present dendritic drainage flow across the

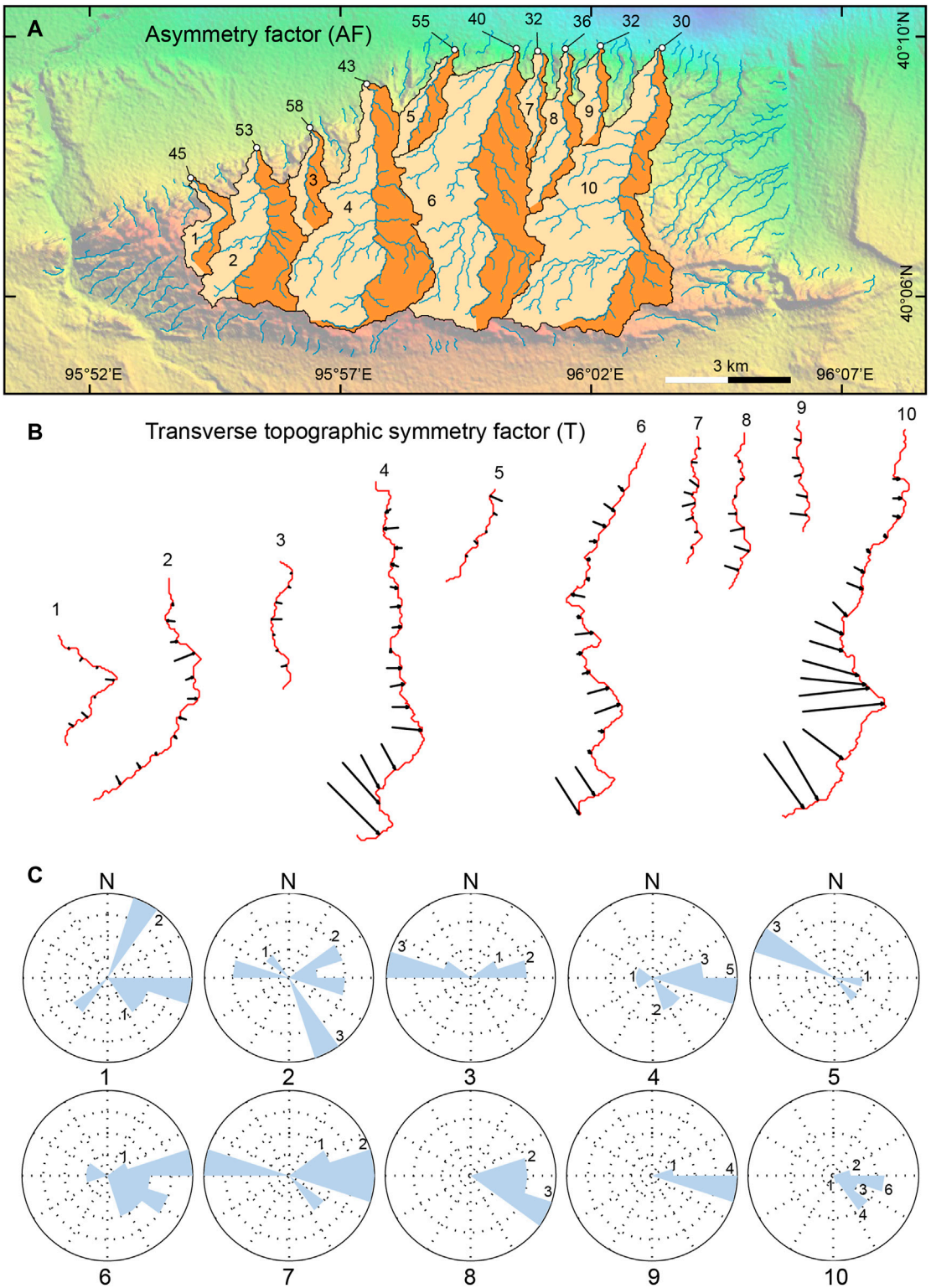

FIGURE 9 | Quantitative morphometric index of the drainage basin on the northern flank of DBTS-C. **(A)** Asymmetry factor (AF) of drainage basin from 1 to 10 outlined in black and the synthetic drainage network shown in blue. **(B)** Trunk river of drainage basin from 1 to 10 showing the migration vector of T in each section. **(C)** Rose and frequency diagram of the T vector.

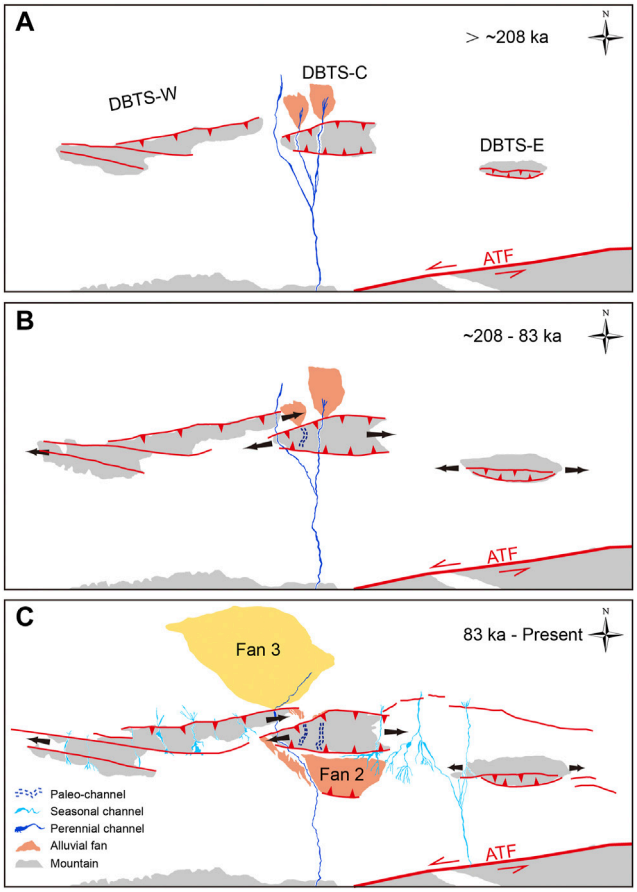

FIGURE 10 | Geomorphic evolution model showing DBTS landscape evolution since ~208 ka. **(A)** In the early stage of ~208 ka, three tributaries flow across DBTS-C on the western flank. **(B)** Accompanied by fold propagation, AG3 was first abandoned at ~208 ka. At ~159 ka, Paleo-terrace T1 was formed by river incision along paleo-river (AG2). **(C)** Until ~83 ka, the incision rate of paleo-river (AG2) cannot keep up with the mountain uplift and the gorge was abandoned on Fan 2 and DBTS-C. The Yulin He would increase its power by accumulating the abandonment flow and deeply incised on alluvial Fans to form a series of terraces since the late-Pleistocene.

Daba sub-basin near Dushanzi (**Figure 2B**), we suppose that the antecedent Yulin He may have a similar pattern.

Figure 10 shows the supposing geomorphic evolution models to illustrate the landform evolution around DBTS since the late mid-Pleistocene. In early 208 ka, the trunk river of the Yulin He flowed across the Daba sub-basin and divided into three tributaries approaching DBTS (**Figure 10A**). All three tributaries flowed across DBTS. Accompanied with the fold propagation of DBTS fault, antecedent river AG3 was firstly abandoned at ~208 ka, leaving two rivers to continue running (**Figure 10B**). At ~159 ka, a continuous incision formed terrace T1 along the alluvial fan and DBTS gorge (AG2). Until ~83 ka, the uplift of F2 and F4 caused the abandonment of the east tributary and left two fault scarps (**Figure 10C**). From then on, only one Yulin He gorge was flowing, and formed Fan 3 and a series of fluvial terraces.

Implications for the Northward Growth of the ATF

Our observations have implications for a new drainage development pattern associated with multi-segment fault growth. Drainages that flow into the bajada could be divided from one stream into several tributaries. Some of the secondary flows have sufficient stream power to cut through propagating anticline and some would have deflected away from the tip. Their abandonment order may not be consistent with the direction of anticline propagation so that the landform relief and stream power would play an important role. Given the fact that the drainages abandoned in an uncommon order, the geomorphic age cannot be used to obtain the fold lateral propagation rate (Bennett et al., 2005). Nevertheless, we could constrain the uplift rate of fault F2 and F4 since ~83 ka, as they deformed the same landscape. Combined with the height of fault scarp, the uplift rate for F2 and F4 since ~83 ka is calculated as 1.24 ± 0.11 and 0.34 ± 0.04 mm/yr, respectively. As we could not obtain the uplift rate of F1, we suggest that the minimum shortening rate across DBTS-C to be ~1.47 mm/yr assuming the fault dips ~47° (Chen, 2018) since ~83 ka. Based on age constraint and displacement measurements, Yang et al., 2020 proposed that the shortening rates in the western and eastern DBTS are approximately 0.3 mm/yr since ~50 ka. A similar shortening rate was also obtained from the deformed terrace along the gorge of Yulin He since ~35.9 ka (Chen et al., 2020). The differences of the shortening rate during the late-Pleistocene indicates that DBTS-C had gone through a relatively severe uplift at ~83 ka.

The fault style, distribution, and deformation pattern along the eastern ATF system has been intensively discussed during the last decade (**Figure 11**) (Yue and Liu, 1999; Zheng et al., 2016; Zhang et al., 2020). To the north of the eastern Altyn Tagh fault there mainly developed the Shanweishan fault and DBTS fault, and to the south developed the Yemahe fault, Daxueshan fault, Yingzuishan fault, Changma fault, and North Qilianshan fault. Several Magnetotelluric and seismic reflection profiles perpendicular across the eastern ATF system indicate that SWSF (Sanweishan fault), DBTSF (Dongbatushan fault), YMHF (Yemahe fault), and YZSF (Yingzuishan fault) are all likely to merge with the ATF at depth of ~30 km (Xiao et al., 2011, 2017; Cunningham et al., 2016; Chen, 2018; Li et al., 2020), and have formed a complex asymmetry flower structure. Yang et al., 2020 used the transgressional duplexing model to illustrate SWSF and NJSF fault kinematics and geometry in the easter ATF. Yun et al., 2020 stated that the Riedel's shear could explain the development of DBTS fault, which stands as the P shear in the model. Their models can well explain the evolution of these faults developed in the shallow lithosphere. However, these secondary faults would merge with the ATF in depth, which may induce the coupling problem between the shallow and deep faults. Based on satellite image of Google earth and seismic reflection profiles, we have found that thrust faults are widely distributed around DBTS, and some are even developed in the Daba sub-basin, such that no sinistral feature has been found since the late mid-Pleistocene. Based on the chronology age of the fault plane and volcanic eruption of

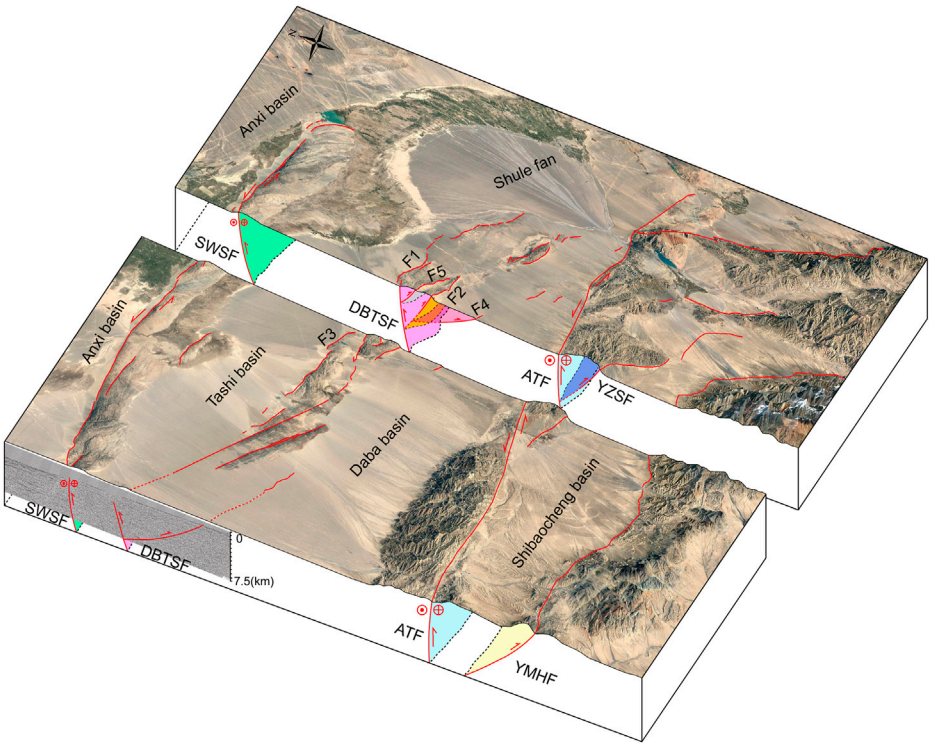

FIGURE 11 | Block diagram with two cross-sections showing downwards projections of sub-parallel faults revealing a flower-like structure along the eastern ATF. The trace of sub-surface fault refers to seismic reflection profiles and magnetotelluric data presented by Chen, 2018 and Xiao et al., 2011.

the Ashkule Volcano Group in west Kunlunshan, Li, 1994 proposed that the ATF had gone through a severe uplift since ~25 ka. Considering the controlling factor of ATF, DBTS region could come under great compression. Thus, we suggest that the pattern of the flower-like structure spreading to both sides under the northward growth of the ATF can better explain the severe uplift of DBTS since ~208 ka.

CONCLUSION

In this study, we investigated the drainage development process and its interaction with the landscape evolution around DBTS based on satellite image interpretation, geomorphic dating, and quantitative geomorphology analysis. We draw the following conclusions:

(1) The course of the Yulin He has gone through several abandonments and left two distinct air gaps along the mountain crestline due to the lateral propagation of DBTS since ~208 ka.
(2) Under multi-segment fault growth and drainage discharge conditions, the direction of drainage abandonment may not be consistent with the fold propagation tendency.
(3) Along the eastern segment of the ATF, the secondary sub-parallel faults developed on both sides of the fault are controlled by a flower-like structure induced by the northward growth of the ATF.

DATA AVAILABILITY STATEMENT

The original contributions presented in the study are included in the article/Supplementary Material, further inquiries can be directed to the corresponding author.

AUTHOR CONTRIBUTIONS

GC did the field work, data processing, and wrote the manuscript. WZ contributed to the conception and provided funding for the study. LD, SL, and JX did the field work. JX, ZL, and LD reviewed and edited the manuscript. All authors contributed to manuscript revision and discussion and approved the submitted version.

FUNDING

This work was supported by the second Tibetan Plateau Scientific Expedition and Research program (STEP) (2019QZKK0901), National Key Research and Development Program of China (2017YFC1500101), the National Science

Foundation of China (41774049, 41874020, 41590861), and Guangdong Province Introduced Innovative R&D Team of Geological Processes and Natural Disasters around the South China Sea (2016ZT06N331).

ACKNOWLEDGMENTS

We would like to express thanks to Yu Zhou for his valuable suggestions.

REFERENCES

Avouac, J.-P., and Tapponnier, P. (1993). Kinematic Model of Active Deformation in central Asia. *Geophys. Res. Lett.* 20 (10), 895–898. doi:10.1029/93GL00128

Balco, G., Stone, J. O., Lifton, N. A., and Dunai, T. J. (2008). A Complete and Easily Accessible Means of Calculating Surface Exposure Ages or Erosion Rates from 10Be and 26Al Measurements. *Quat. Geochronol.* 3 (3), 174–195. doi:10.1016/j.quageo.2007.12.001

Bennett, E. R., Youngson, J. H., Jackson, J. A., Norris, R. J., Raisbeck, G. M., Yiou, F., et al. (2005). Growth of South Rough Ridge, Central Otago, New Zealand: Using *In Situ* Cosmogenic Isotopes and Geomorphology to Study an Active, Blind Reverse Fault. *J. Geophys. Res. Solid Earth* 110 (B2). doi:10.1029/2004JB003184

Bretis, B., Bartl, N., and Grasemann, B. (2011). Lateral Fold Growth and Linkage in the Zagros Fold and Thrust belt (Kurdistan, NE Iraq). *Basin Res.* 23 (6), 615–630. doi:10.1111/j.1365-2117.2011.00506.x

Burbank, D. W., and Anderson, R. S. (2001). *Tectonic Geomorphology*. Massachusetts: Blackwell Science. doi:10.1002/9781444345063

Chen, G., Zheng, W., Xiong, J., Zhang, P. Z., Li, Z. G., and Yu, J. X. (2020). Late Quaternary Fluvial Landform Evolution and Controlling Factors along the Yulin River on the Northern Tibetan Plateau. *Geomorphology* 363, 107213. doi:10.1016/j.geomorph.2020.107213

Chen, G. (2018). *The Evolution of the Yulin River and its Defomation to the Northwestward Growth of the Altyn Tagh Fault*. Beijing: Institute of Geology, China Earthquake Administration. Master thesis.

Collignon, M., Fernandez, N., and Kaus, B. J. P. (2015). Influence of Surface Processes and Initial Topography on Lateral Fold Growth and Fold Linkage Mode. *Tectonics* 34 (7-8), 1622–1645. doi:10.1002/2015TC003843

Cowgill, E., Yin, A., Wang, X. F., and Zhang, Q. (2000). Is the North Altyn Fault Part of a Strike-Slip Duplex along the Altyn Tagh Fault System? *Geology* 28 (3), 255–258. doi:10.1130/0091-7613(2000)028<0255:itnafp>2.3.co;2

Cowgill, E., Gold, R. D., Xuanhua, C., Xiaofeng, W., Arrowsmith, J. R., and Southon, J. (2009). Low Quaternary Slip Rate Reconciles Geodetic and Geologic Rates along the Altyn Tagh Fault, Northwestern Tibet. *Geology* 37 (7), 647–650. doi:10.1130/G25623A.1

Cowgill, E. (2007). Impact of Riser Reconstructions on Estimation of Secular Variation in Rates of Strike-Slip Faulting: Revisiting the Cherchen River Site along the Altyn Tagh Fault, NW China. *Earth Planet. Sci. Lett.* 254 (3–4), 239–255. doi:10.1016/j.epsl.2006.09.015

Cox, R. T. (1994). Analysis of Drainage-basin Symmetry as a Rapid Technique to Identify Areas of Possible Quaternary Tilt-Block Tectonics: an Example from the Mississippi Embayment. *GSA Bull.* 106 (5), 571–581. doi:10.1130/0016-7606(1994)106<0571:aodbsa>2.3.co;2

Cunningham, D., Zhang, J., and Li, Y. (2016). Late Cenozoic Transpressional Mountain Building Directly north of the Altyn Tagh Fault in the Sanweishan and Nanjieshan, North Tibetan Foreland, China. *Tectonophysics* 687, 111–128. doi:10.1016/j.tecto.2016.09.010

Deng, Q. D., Zhang, P. Z., Ran, Y. K., Min, W., Yang, X. P., and Chu, Q. Z. (2003). Basic Characteristics of Active Tectonics of China. *Sci. China Ser. D Earth Sci.* 46 (4), 357–372. (in Chinese with English abstract). doi:10.1360/03yd9032

Ellis, M. A., and Barnes, J. B. (2015). A Global Perspective on the Topographic Response to Fault Growth. *Geosphere* 11 (4), 1008–1023. doi:10.1130/GES01156.1

Gold, R. D., Cowgill, E., Arrowsmith, J. R., Gosse, J., Chen, X., and Wang, X. F. (2009). Riser Diachroneity, Lateral Erosion, and Uncertainty in Rates of Strike-Slip Faulting: A Case Study from Tuzidun along the Altyn Tagh Fault, NW China. *J. Geophys. Res.–Solid Earth* 114 (B4), B04401. doi:10.1029/2008JB005913

Gosse, J. C., and Phillips, F. M. (2001). Terrestrial *In Situ* Cosmogenic Nuclides Theory and Application. *Quat. Sci. Rev.* 20 (14), 1475–1560. doi:10.1016/S0277-3791(00)00171-2

Grasemann, B., and Schmalholz, S. M. (2012). Lateral Fold Growth and Fold Linkage. *Geology* 40 (11), 1039–1042. doi:10.1130/G33613.1

Hare, P. H., and Gardner, T. W. (1985). "Geomorphic Indicators of Vertical Neotectonism along Converging Plate Margins, Nicoya Peninsula, Costa Rica," in *Tectonic Geomorphology*. Editors M Morisawa and J. T Hack (Boston: Allen & Unwin), 75–104.

He, Z. Y., Zhang, Z. M., Zong, K. Q., and Dong, X. (2013). Paleoproterozoic Crustal Evolution of the Tarim Craton: Constrained by Zircon U-Pb and Hf Isotopes of Meta-Igneous Rocks from Korla and Dunhuang. *J. Asian Earth Sci.* 78, 54–70. doi:10.1016/j.jseaes.2013.07.022

Hetzel, R., Tao, M., Niedermann, S., Strecker, M., Ivy-Ochs, S., and Kubik, P. W. (2004). Implications of the Fault Scaling Law for the Growth of Topography: Mountain Ranges in the Broken Foreland of north-east Tibet. *Terra Nova* 16, 157–162. doi:10.1111/j.1365-3121.2004.00549.x

Jackson, J., Ritz, J. F., Siame, L., Raisbeck, G., Yiou, F., and Norris, R. (2002). Fault Growth and Landscape Development Rates in Otago, New Zealand, Using *In Situ* Cosmogenic ^{10}Be. *Earth Planet. Sci. Lett.* 195, 185–193. doi:10.1016/S0012-821X(01)00583-0

Keller, E. A., and DeVecchio, D. E. (2013). "Tectonic Geomorphology of Active Folding and Development of Transverse Drainages," in *Treatise on Geomorphology* (Elsevier), 129–147. doi:10.1016/B978-0-12-374739-6.00088-9

Keller, E. A., Zepeda, R. L., Rockwell, T. K., Ku, T. L., and Dinklage, W. S. (1998). Active Tectonics at Wheeler Ridge, Southern San Joaquin Valley, California. *Geol. Soc. Am. Bull.* 110, 298–310. doi:10.1130/0016-7606(1998)110<0298:atawrs>2.3.co;2

Keller, E. A., Gurrola, L., and Tierney, T. E. (1999). Geomorphic Criteria to Determine Direction of Lateral Propagation of Reverse Faulting and Folding. *Geology* 27, 515–518. doi:10.1130/0091-7613(1999)027<0515:gctddo>2.3.co;2

Lacombe, O., Roure, F., and Lavé, J. (2007). Thrust Belts and Foreland Basins: From Fold Kinematics to Hydrocarbon Systems. *Front. Earth Sci.* 14 (5), 205–228. doi:10.1007/978-3-540-69426-7

Lal, D. (1991). Cosmic ray Labeling of Erosion Surfaces *In Situ* Nuclide Production Rates and Erosion Models. *Earth Planet. Sci. Lett.* 104, 424–439. doi:10.1016/0012-821X(91)90220-C

Li, M., Xiao, Q. B., and Yu, G. (2020). Electrical Structure of the Altyn Tagh Fault at the Changma Section and its Tectonic Significance. *Chin. J. Geophys.* 63 (11), 4125–4143. doi:10.6038/cjg2020N0413

Li, Z. Z. (1994). Formation and Evolution of the Tectonic Landforms in the Altun Mountain and its Neighboring Region. *Geogr. Res.* 13 (3), 35–42.

Liu, J., Ren, Z., Zheng, W., Min, W., Li, Z., and Zheng, G. (2020). Late Quaternary Slip Rate of the Aksay Segment and its Rapidly Decreasing Gradient along the Altyn Tagh Fault. *Geosphere* 16 (6), 1538–1557. doi:10.1130/GES02250.1

Molnar, P., and Tapponnier, P. (1975). Cenozoic Tectonics of Asia: Effects of a continental Collision: Features of Recent continental Tectonics in Asia Can Be Interpreted as Results of the India-Eurasia Collision. *Science* 189 (4201), 419–426. doi:10.1126/science.189.4201.419

Ramsey, L. A., Walker, R. T., and Jackson, J. (2007). Geomorphic Constraints on the Active Tectonics of Southern Taiwan. *Geophys. J. Int.* 170 (3), 1357–1372. doi:10.1111/j.1365-246X.2007.03444.x

Ramsey, L. A., Walker, R. T., and Jackson, J. (2008). Fold Evolution and Drainage Development in the Zagros Mountains of Fars Province, SE Iran. *Basin Res.* 20 (1), 23–48. doi:10.1111/j.1365-2117.2007.00342.x

Salvany, J. M. (2004). Tilting Neotectonics of the Guadiamar Drainage basin, SW Spain. *Earth Surf. Process. Landforms* 29 (2), 145–160. doi:10.1002/esp.1005

Schumm, S. A., Dumont, J. F., and Holbrook, J. M. (2000). *Active Tectonics and Alluvial Rivers*. Cambridge: Cambridge University Press.

Shahzad, F., and Gloaguen, R. (2011). TecDEM: A MATLAB Based Toolbox for Tectonic Geomorphology, Part 2: Surface Dynamics and Basin Analysis. *Comput. Geosci.* 37 (2), 261–271.

Stone, J. O. (2000). Air Pressure and Cosmogenic Isotope Production. *J. Geophys. Res.* 105, 23753–23759. doi:10.1029/2000JB900181

Tapponnier, P., Zhiqin, X., Roger, F., Meyer, B., Arnaud, N., and Wittlinger, G. (2001). Oblique Stepwise Rise and Growth of the Tibet Plateau. *Science* 294 (5547), 1671–1677. doi:10.1126/science.105978

Wang, P., Lu, Y., Ding, G., Chen, J., and Wyrwoll, K. H. (2004). Response of the Development of the Shule River Alluvial Fan to Tectonic Activity. *Quat. Sci.* 24 (1), 74–81. (in Chinese with English abstract). doi:10.3969/j.issn.0253-4967.2004.04.017

Wang, H. Y. C., Wang, J., Wang, G. D., Lu, J. S., Chen, H. X., and Peng, T. (2017). Metamorphic Evolution and Geochronology of the Dunhuang Orogenic belt in the Hongliuxia Area, Northwestern China. *J. Asian Earth Sci.* 135, 51–69. doi:10.1016/j.jseaes.2016.12.014

Wang, Y. T. (1989). The Research of Quaternary basin of Dunhuang in the Western Gansu. *Gansu Geol.* (10), 39–55. (in Chinese with English abstract).

Xiao, Q., Zhao, G., and Dong, Z. (2011). Electrical Resistivity Structure at the Northern Margin of the Tibetan Plateau and Tectonic Implications. *J. Geophys. Res. Solid Earth* 116 (B12). doi:10.1029/2010JB008163

Xiao, Q., Shao, G., Liu-Zeng, J., Oskin, M. E., Zhang, J., and Zhao, G. (2015). Eastern Termination of the Altyn Tagh Fault, Western China: Constraints from a Magnetotelluric Survey. *J. Geophys. Res. Solid Earth* 120 (5), 2838–2858. doi:10.1002/2014JB011363

Xiao, Q., Yu, G., Liu-Zeng, J., Oskin, M. E., and Shao, G. (2017). Structure and Geometry of the Aksay Restraining Double bend along the Altyn Tagh Fault, Northern Tibet, Imaged Using Magnetotelluric Method. *Geophys. Res. Lett.* 44 (9), 4090–4097. doi:10.1002/2017GL072581

Xu, X., Wang, F., Zheng, R., Chen, W., Ma, W., Yu, G., et al. (2005). Late Quaternary Sinistral Slip Rate Along the Altyn Tagh Fault and Its Structural Transformation Model. *Sci. China Ser. D* 48 (3), 14. doi:10.1360/02yd0436

Yang, H., Yang, X., Cunningham, D., Hu, Z., Huang, X., and Huang, W. (2020). A Regionally Evolving Transpressional Duplex along the Northern Margin of the Altyn Tagh Fault: New Kinematic and Timing Constraints from the Sanweishan and Nanjieshan, China. *Tectonics* 39 (2). doi:10.1029/2019tc005749

Yin, A., Rumelhart, P. E., Butler, R., Cowgill, E., Harrison, T. M., and Foster, D. A. (2002). Tectonic History of the Altyn Tagh Fault System in Northern Tibet Inferred from Cenozoic Sedimentation. *Geol. Soc. Am. Bull.* 114, 1257–1295. doi:10.1130/0016-7606(2002)114<1257:thotat>2.0.co;2

Yue, Y., and Liu, J. G. (1999). Two-stage Evolution Model for the Altyn Tagh Fault, China. *Geology* 27 (3), 227–230. doi:10.1130/0091-10.1130/0091-7613(1999)027<0227:tsemft>2.3.co;2

Yun, L., Zhang, J., Wang, J., Yang, X. P., Qu, J. F., and Zhang, B. H. (2020). Active Deformation to the north of the Altyn Tagh Fault: Constraints on the Northward Growth of the Northern Tibetan Plateau. *J. Asian Earth Sci.* 198, 104312. doi:10.1016/j.jseaes.2020.104312

Zhang, P. Z., Molnar, P., and Xu, X. (2007). Late Quaternary and Present-Day Rates of Slip along the Altyn Tagh Fault, Northern Margin of the Tibetan Plateau. *Tectonics* 26 (5), TC5010.1–TC5010.24. doi:10.1029/2006TC002014

Zhang, J., Yun, L., Zhang, B., Qu, J. F., Zhao, H., and Hui, J. (2020). Deformation at the Easternmost Altyn Tagh Fault: Constraints on the Growth of the Northern Qinghai–Tibetan Plateau. *Acta Geol. Sin.-English Ed.* 94 (4), 988–1006. doi:10.1111/1755-6724.14555

Zhao, Y., Diwu, C., Ao, W., Wang, H., Zhu, T., and Sun, Y. (2015). Ca. 3.06 Ga Granodioritic Gneiss in Dunhuang Block. *Chin. Sci. Bull. (Chin. Vers.)* 60 (1), 75–87. (in Chinese). doi:10.1360/n972014-00382

Zheng, W. J., Zhang, P. Z., He, W. G., Yuan, D. Y., Shao, Y. X., and Zheng, D. W. (2013). Transformation of Displacement between Strike-Slip and Crustal Shortening in the Northern Margin of the Tibetan Plateau: Evidence from Decadal GPS Measurements and Late Quaternary Slip Rates on Faults. *Tectonophysics* 584, 267–280. doi:10.1016/j.tecto.2012.01.006

Zheng, W. J., Yuan, D. Y., Zhang, P. Z., Yu, J. X., Lei, Q. Y., and Wang, W. T. (2016). Tectonic Geometry and Kinematic Dissipation of the Active Faults in the Northeastern Tibetan Plateau and Their Implications for Understanding Northeastward Growth of the Plateau. *Quat. Sci.* 34 (4), 775–788. (in Chinese).

Zhuang, G. S., Hourigan, J. K., Ritts, B. D., and Kent-Corson, M. L. (2011). Cenozoic Multiple-phase Tectonic Evolution of the Northern Tibetan Plateau: Constraints from Sedimentary Records from Qaidam basin, Hexi Corridor, and Subei basin, Northwest China. *Am. J. Sci.* 311 (2), 116–152. doi:10.2475/02.2011.02

Conflict of Interest: The authors declare that the research was conducted in the absence of any commercial or financial relationships that could be construed as a potential conflict of interest.